A Simulation of Surface Runoff and Infiltration due to Torrential Rainfall Based on Field Monitoring Results at a Slope Comprising Weathered Granite

H. Ohtsu[1], H. Masuda[2], T. Kitaoka[3], K. Takahashi[4], M. Yabe[5], S. Soralump[6] and Y. Maeda[7]
[1,2,3]*Department of Urban Management, Graduate School of Engineering, Kyoto University, Kyoto, Japan*
[4]*Water Resource Consultant, Chiba, Japan*
[5]*Oyo Corporation, Tokyo, Japan*
[6]*Department of Civil Engineering, Kasetsart University, Bangkok, Thailand*
[7]*Department of Engineering, West Nippon Expressway Company Limited, Osaka, Japan*
[1,2,3]*E-mail*: hiroyasu.ohtsu.6n@ kyoto-u.ac.jp, masuda.hiroshi.64s@st.kyoto-u.ac.jp, kitaoka.takafumi.6e@kyoto-u.ac.jp
[4]*E-mail*: takahashi@hydrology-tec.com
[5]*E-mail:* yabe-mituru@oyonet.oyo.co.jp
[6]*E-mail*: fengsus@ku.ac.th
[7]*E-mail*: y.maeda.ac@w-nexco.co.jp

ABSTRACT: The frequency of rainfall-triggered slope failure has recently been increasing in Asian countries. One plausible reason for the increased frequency is climate change. It is therefore a pressing issue to clarify the mechanism of infiltration, causing slope failure. From such a viewpoint, this study investigated the relationship of the runoff, the infiltration and the surface retention due to torrential rainfall by means of one-dimensional tank model analysis using the results of field measurement conducted in Phuket, Thailand. The results showed that the infiltration is temporally retained by the surface retention at the beginning of rainfall, including immediately after and that the time rate of the infiltration is affected by the rainfall intensity. Furthermore, this study investigated the applicability of the proposed method, which deals with the infiltration simulated by one-dimensional tank model analysis, by comparing with the measured values and the results of conventional method.

Keywords: Slope, Seepage analysis, One-dimensional tank model

1. INTRODUCTION

Recently, the frequency of rainfall-triggered slope failure has drastically been increasing in Asian countries. The increase in frequency has been attributed to climate change. It is generally well-known that rainfall-triggered slope failure takes place in relatively shallow portions of slopes (Phien-Wej et al, 1993; Soralump, 2010). Therefore, it is necessary to investigate the rainfall-infiltration (runoff) characteristics in unsaturated soil near the slope surface.

Generally, the moisture in unsaturated soil has a non-linear relationship with suction and exhibits hysteresis. The relationship is known as the soil water characteristic curve (hereafter, referred to as "SWCC") (e.g. Fredlund & Rahardjo, 1993). However, SWCCs in the field are different from those in laboratory test since they are generally corresponding to a scanning-curve lying between original wetting-drying curves and the soil in the field is always under the load from the soil above and confined by its surrounding soil (Bujang et al, 2005).

If evapotranspiration is ignored, the rainfall near the slope surface can be divided into initial abstraction, infiltration and runoff. It is well-know that there are close correlation among the components. For an example, runoff is produced only when rainfall intensity exceeds infiltration capacity as shown in Figure 1 (Horton, 1940). Accurate runoff measurement in the field can be made in contrast to the determination of other components (Premchitt et al, 1992). Therefore, extensive field measurement programs have been carried out (e.g. Premchitt et al, 1992; Matsushi, 2006). The production of runoff is generally affected by many factors as follows: geological condition (permeability of soil), rainfall characteristics (rainfall amount, rainfall intensity, rainfall duration, and antecedent rainfall), type of soil cover (vegetation) and so on. Premchitt et al (1992) conducted filed measurement on the runoff at seven man-made slopes with various types of surface cover. The results revealed that the runoff is largely dependent on the rainfall amount, while other parameters such as antecedent rainfall and duration contribute small secondary effects.

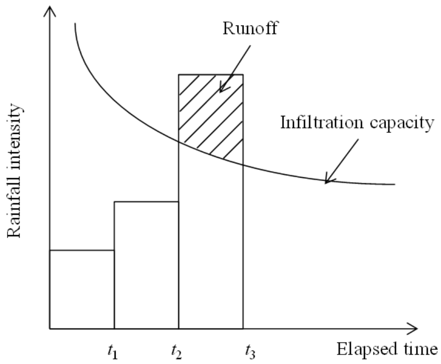

Figure 1 Correlation of runoff and infiltration capacity

In this study, a one-dimensional tank model is adopted for the simulation to clarify the rainfall-runoff relationship near the slope surface. The procedure can be summarized as follows: first, the parameters for the model are identified by performing inverse analysis based on the one-dimensional tank model using the Kalman filter, with the runoff data measured at the actual site (Suwanishwong et al, 2008). Then, forward analysis is performed using the identified parameters to clarify the relationship between the infiltration and the temporary retained amount near the surface (hereafter, referred as the "surface retention").

In contrast, for the analyses on rainfall-infiltration characteristics in the slope by means of numerical analysis, there have been many saturated-unsaturated seepage analyses formulated by the finite element method. The study by Neuman (1974) can be considered as a representative one. In the method, the infiltration is calculated by iterative calculations, in which boundary conditions are determined through trial and error (hereafter, referred as "the conventional method"). In this study, the method to deal with the infiltration calculated by the analysis of the one-dimensional model as a prescribed flux boundary is proposed. Finally, the applicability of the proposed method is investigated by comparing with the measured valued and the result of the conventional method.

2. OVERVIEW OF THE SITE FOR FIELD MEARSUREMENT

The slope in this study is located along a highway (Highway No, 4028) in Phuket, Thailand about 600 km south of Bangkok. It is a weathered granite cut slope with grass cover with an average gradient about "1:1.3" (Vertical: Horizontal), that is, about 37.5 degrees (Ohtsu, et al, 2013).

2.1 Geological and soil conditions

Figure 2 shows the survey lines A to D and 1 to 4 in the slope, in which various field investigation (e. g., topographical survey, electrical prospecting and penetration test) were carried out and the in-situ samples for laboratory tests were collected.

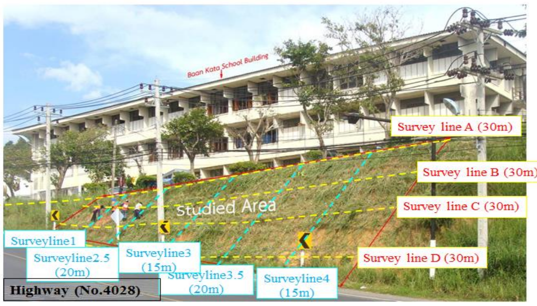

Figure 2 Field monitoring survey lines

Figure 3 shows the results of electrical prospecting for the survey line A, survey lines 3 and 4, respectively. The results indicate that the granite weathering advanced up to 7 to 8m from the slope surface, and that the distribution of electrical resistivity is very complex, reflecting the variability of degree of weathering at the slope. According to previous research works (Little, 1969, Dearman et al, 1978, GCO, 1984), the weathering profile for granite is generally divided into six ranks, I to VI. While the slightly weathered and moderately weathered zones (grade II and III) tend to behave in engineering terms as rock as well as the fresh bedrock (grade I), weathered granite of grade V to VI tends to behave in engineering terms as soil (Geological Society Engineering Group, 1994). It can be considered that in accordance with the above classifications, the portion with the resistivity ranging from 15 to 865 Ωm is either residual soil or weathered granite (Rank V to VI), whereas that of over 865 Ωm is less-weathered granite (Rank IV to III). In addition, the portions with higher resistivity locally observed in the relatively shallow portion can be interpreted as boulders (core stones) as shown in Figure 3.

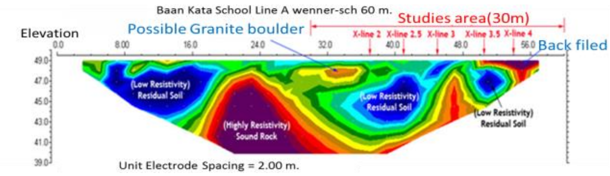

(a) Resistivity at survey line A

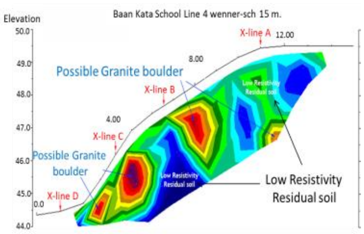

(b) Resistivity at survey line 3

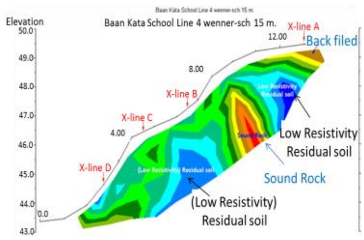

(c) Resistivity at survey line 4

Figure 3 Results of electrical prospecting

Figure 4 shows the grain size distribution curves for weathered granite (grade V to VI) collected at the depth of 0.0 to 4.0m of the survey lines 3 and 4 by hand auger. It indicates that the coarser component (sand & gravel) is dominant in the geological composition of the slope from the slope surface to the deep portion.

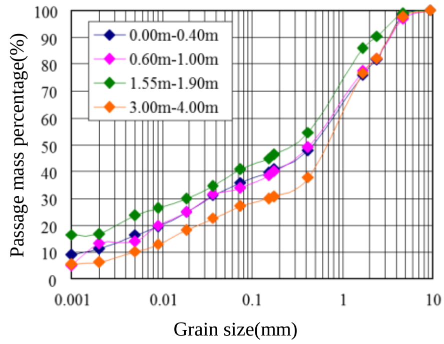

(a)B 3

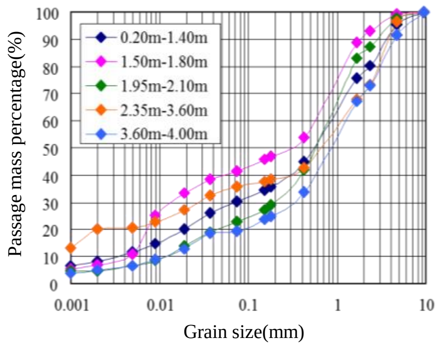

(b) B4

Figure 4 Grain size distribution curve

In general, the finer fraction is a secondary product of weathering (Jworchan, 2006). Figure 5 shows the histograms of the clay and silt contents for the in-situ samples. The clay content varies from 4% to 21% and the average value is 10%, while the silt content varies from 2% to 22% and the average value is 9%. While both clay and silt contents for samples are mostly 5-10%, those for a few samples are 15% over. It appears to reflect the variability of degree of weathering shown in Figure 3.

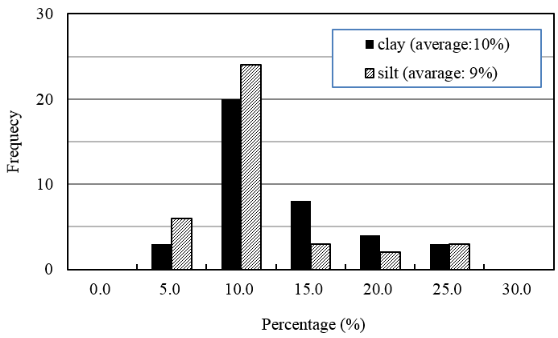

Figure 5 Histograms of the clay and silt contents

In addition, 12 undisturbed samples for the laboratory test to obtain SWCCs were collected from two trial pits (TP1 & TP2) shown in Figure 6. Table 1 shows the results of void ratio e and degree of saturation S_r for the samples. On average the void ration is between 0.3 and 0.8 except for PK-18 & PK-20 at TP2. It can be considered that the deviation of void ratio from average value reflect the variability of degree of weathering as well as that of the finer fraction shown Figure 5. The degree of saturation is mostly between 0.3 and 0.7. It is therefore considered that physical properties at the slope show no strong dependence on depth.

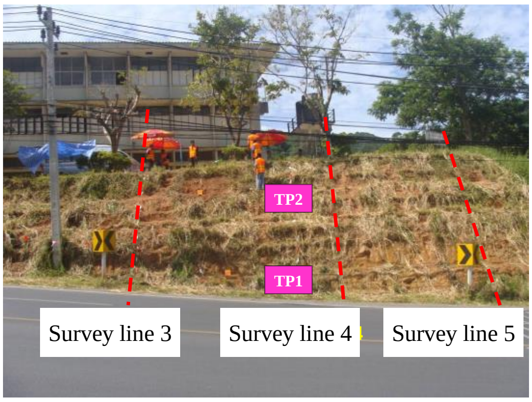

Figure 6 Location of trial pits

Table.1 Soil properties

Specimen	Depth (m)	Void ratio e	ρ_s (g/cm^3)	S_r	γ_{sat} (kN/m^3)
PK-01(TP2)	0.40	0.66	2.50	0.65	17.60
PK-04(TP2)	0.40	0.71	2.60	0.40	16.90
PK-12(TP2)	0.60	0.74	2.50	0.47	16.30
PK-13(TP2)	0.60	0.73	2.50	0.44	16.30
PK-18(TP2)	1.00	0.83	2.50	0.38	15.40
PK-20(TP2)	1.00	0.90	2.50	0.30	14.60
PK-25(TP1)	0.40	0.63	2.50	0.49	17.20
PK-32(TP1)	0.40	0.56	2.50	0.56	18.00
PK-33(TP1)	0.60	0.58	2.50	0.63	18.10
PK-40(TP1)	0.60	0.54	2.50	0.64	18.50
PK-41(TP1)	1.00	0.78	2.50	0.47	16.10
PK-48(TP1)	1.00	0.59	2.50	0.63	18.10

Figure 7 shows the SWCCs for PK-13 & PK-32. It is observed that the results show hysteretic behaviour between the wetting and drying curves as well as past research works (e.g. Fredlund & Rahardjo, 1993).

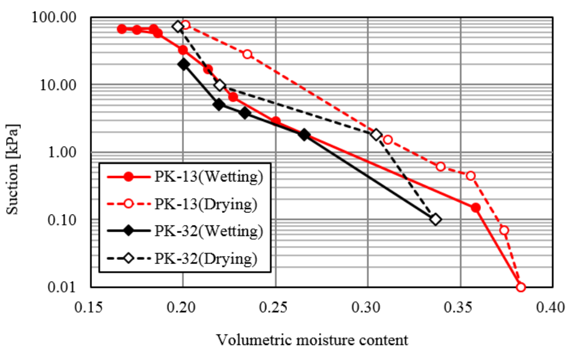

Figure 7 Soil moisture characteristic curves

Furthermore, two types of in-situ tests were conducted in order to obtain the saturated coefficient of permeability of the slope. One is the borehole permeameter method and the other is a simplified test using an acrylic pipe and a compact water-level gauge to define the infiltration from the slope surface by measuring the water level. Table 2 shows the saturated coefficient of permeability obtained by both methods. The results that the saturated coefficient of permeability of the ground surface was relatively high from 10^{-4} to 10^{-6} *m/s* and reduced a little at the depth of 2 to 3m (10^{-6}*m/s*) show good agreement with the above finding that the coarser component is dominant in the textural composition shown in Figure 5.

Table 2 Saturated coefficient of permeability

Borehole permeameter method	Top of slope (GL-2.92m)	6.79×10^{-6} m/sec
	Toe of slope (GL-2.26m)	5.48×10^{-6} m/sec
Surface infiltration experiment	Top of slope area	1.51×10^{-4}m/sec
	Middle of slope area 1	7.22×10^{-5}m/sec
	Middle of slope area 2	1.74×10^{-5}m/sec
	Toe of slope area	1.15×10^{-4}m/sec

2. 2 Layout of measuring instruments

This section outlines the field measurement system of the slope. First, Figure 8 shows the cross-section view and the plan view of the layout of instruments, in addition to the geological condition. As Figure 8 indicates, based on the previously described results of the electrical prospecting as well as the penetration test, the geological conditions at the measurement site can be classified into Rank VI (residual soil), Rank V (completely weathered) and Rank IV (highly weathered) according to the classification suggested by Little (1969), at the depths of approximately 1.0m, from 1.0m to 4.0m and over 4.0m, respectively.

For the field measurement in the slope, a tipping rainfall gauge and Palmer-Bowlus Flume (hereafter, referred as “PB flume”) were installed to monitor the rainfall-runoff characteristic, and tensiometers and moisture meters were installed to monitor the rainfall-infiltration characteristic.

The Palmer-Bowlus Flume (hereafter, called “PB-flume”) is a sensor system to measure water level of a ditch, which is converted to runoff. The dimensions of the PB-flume installed in the slope was shown in Figure 9, and the measured water level H_u is converted to the runoff for the area of the catchment in the slope (30.15m^2) in accordance with the following equations:

$$H_u = 173.64 - X + 16.7 \quad (1)$$

$$Q_R = 0.0531 \cdot H_u{}^2 - 1.8009 H_u + 16.06 \quad (2)$$

The tensiometer, which was developed to evaluate the water retention characteristics of soil for agriculture (Inoe, 1994), has a system to compensate for atmosphere pressure and is capable of measuring the pore-water pressure ranging from 100 to -100 kPa. It has a pressure sensor at the measuring unit that can receive little influence from changes of ground temperature on the suction measurements with a precision of ±0.5kPa or smaller.

On the other hand, for volumetric water content, the dielectric constant-type (EC-5 manufactured by DECAGON) soil moisture meter was used. The moisture meter has different calibration equations of the “dielectric constant – volumetric water content” for different types of soil. Therefore, in this study, based on the correlation of the measured voltage and the moisture volumetric content for the in-situ soil samples shown in Figure 10, the content for the in-situ soil samples shown in Figure 10, the following calibration equation was obtained:

$$\theta = 14.78V^5 - 47.33V^4 + 53.63V^3 - 25.66V^2 + 5.43V - 0.33 \quad (3)$$

In which, V denotes measured voltage and θ denotes volumetric moisture content.

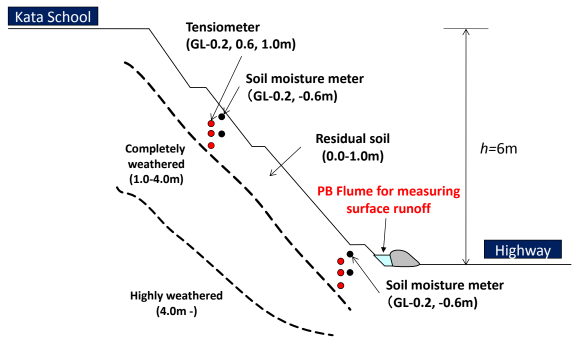

(a) Cross-section view of slope

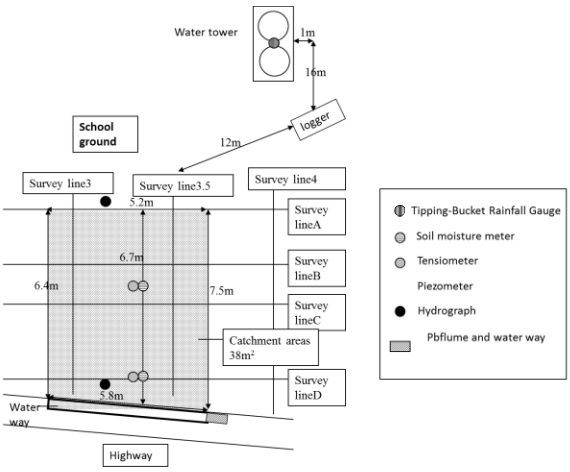

(b) Plan view of slope

Figure 8 Location of trial pits

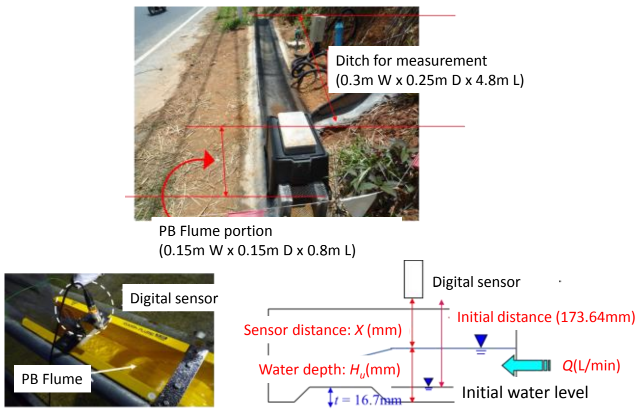

Figure 9 PB flume and measurement system of runoff

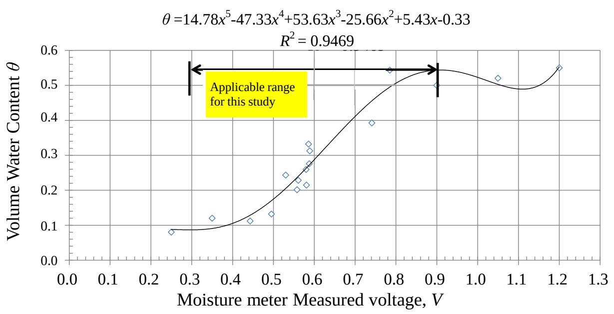

Figure 10 Correlation of the measured voltage and the moisture volumetric content for in-situ samples

3. RESULTS OF FIELD MEASUREMENT

3.1 Runoff

The data (shown as P-site in the figure) obtained in this study are shown in Figure 11 (a) and (b). In the figures, the data (shown as H-site in the figure) ,which was obtained at the weathered granite cut slope with grass in Hong Kong by Premchitt et al (1992), are also plotted for comparison and SCS curves (SCS, 1972) are also drawn for each slope to define the envelopes which contain most of data points. As shown in Figure 11(a), while the runoff ratios for each slope at smaller rainfall, which is the ratio of the runoff to the rainfall amount, are relatively small and scattered, they tend to converge to certain values at high rainfall. The slope in this study had the smaller average runoff ratio of 0.20, in comparison with the average runoff ratio of 0.27 for H-site. In a same manner, as shown in Figure 11(b), for the slope in this study, the data are within the CN values 80 and 50, in comparison with the CN values 85 and 55 for the slope at H-site. The results indicate that the rainfall-runoff relationships for the slope in this study are very similar to those for the slope at H-site, and the permeability for the slope in this study is a little bit higher than that for H-site slope.

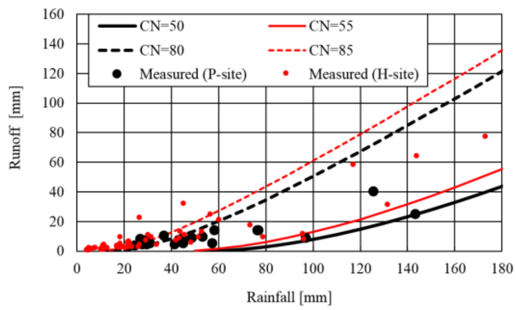

(a) Rainfall and runoff

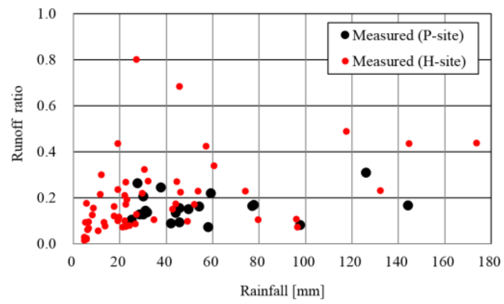

(b) Rainfall and runoff ratio

Figure 11 Rainfall-runoff characteristics

3.2 Comparison of Field and Laboratory Data on SWCCs

Figure 12 shows the combined plot of the field pore-water pressure, laboratory suction and volumetric moisture content for both the middle portion and slope toe. In Figure 12, the van Genuchten's soil water retention curves (van Genuchten, 1980) for the in-situ sample date PK-01, PK-12, PK-25 and PK-32 are drawn. The van Genuchten's soil water retention curve method is described as follows:

$$S_e = \frac{\theta - \theta_r}{\theta_s - \theta_r} = \left[\frac{1}{1 + (\alpha \times h_e)^n} \right]^m \tag{4}$$

$$m = 1 - \frac{1}{n} \tag{5}$$

In which, S_e denotes effective saturation, θ denotes volumetric moisture content, θ_s denotes saturated volumetric moisture content, θ_r denotes residual volumetric moisture content, h_e denotes pressure head, and α, n, m denote experimental constants. In this study, the experimental constants for van Genuchten model (hereafter, referred as "VG model") were identified by "SWRC-Fitting program" (Seki, 2007).

As described by Bujang et al (2005), the comparison between the field and laboratory measurements inevitably involve different degree of disturbance that can have significant influence on the soil behavior, and the soil in the field has always been under the load from the soil above and confined by its surrounding soil.

In Figure 12, because the field measurement in this study was conducted during rainy season, the values of suction were relatively small and the significant hysteric behavior of the SWCCs was not observed. In the comparison of the values for the middle portion, while the shape of the field (wetting) curves is relatively similar to that for in-situ sample date PK-01, the values of suction/pore-water pressure at any particular moisture content are mostly different and the saturated volumetric moisture contents for the field measurement are smaller than those for the laboratory test. On the other hand, in the comparison of the values for the slope toe, the shape of the field (wetting) curves at GL-0.6m is very similar to those of the laboratory tests. However, the saturated volumetric moisture contents for the field measurement are smaller than those for the laboratory test as well as those for the middle portion. It can be considered that the confined pressure by surrounding soil has an effect in pushing down the SWCCs (Bujang et al, 2005).

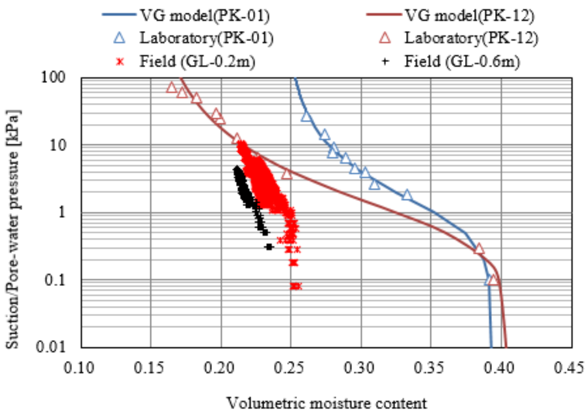

(a) Middle portion

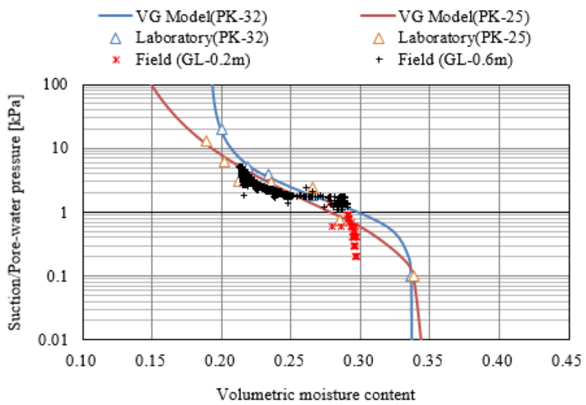

(b) Slope toe

Figure 12 Combined plot of the field, laboratory suction/pore-water pressure and volumetric moisture content

4. SIMULATION USING ONE-DIMENSIONAL TANK MODEL

4.1 Overview of simulation

Sugawara (1995) developed Multi-Tank Model system to calculate surface runoff, interflow and groundwater flow for relatively large catchments in a simple manner. However, this study focuses on the runoff and the infiltration, which is locally retained for a small catchment are discussed. Therefore, in this study, the one-dimensional tank model shown in Figure 13 was developed. In the tank model, it is assumed that rainfall is divided into three parts: the runoff, the infiltration, and the surface retention, which is retained at the slope surface at the beginning of the rainfall and is partially transferred to the infiltration subsequently.

In the tank model, the time rates of runoff $q_R(t)$ and infiltration $q_I(t)$ at a time t are defined by equation (6) and equation (7), respectively:

$$\begin{array}{lll} If & X(t)-H \le 0, & q_r(t)=0 \\ If & X(t)-H > 0, & q_r(t)=\alpha\cdot[X(t)-H] \end{array} \tag{6}$$

$$q_I(t)=b\cdot X(t) \tag{7}$$

In which, $X(t)$ is the height of the retained water in a tank at a time t, H is the height to the outflow vent, a is the coefficient of runoff and b is the coefficient of infiltration. Both a and b have the dimension of T^{-1} (T: time). Among the parameters, the height to the outflow vent, H indicates the cumulated rainfall before the runoff is produced. It can be defined based on the correlation between the cumulative amounts of runoff and rainfall measured at the slope.

Based on the above conditions, the equation of continuity shown in Figure 13 should be as follows:

$$\frac{dX(t)}{dt}=P(t)-a\cdot[X(t)-H]-b\cdot X(t) \tag{8}$$

In this study, the coefficients of runoff and infiltration involved in the equations from (6) to (8) are identified by inverse analysis using the Kalman filter (Suwanishwong et al, 2008). The procedure for which is described below.

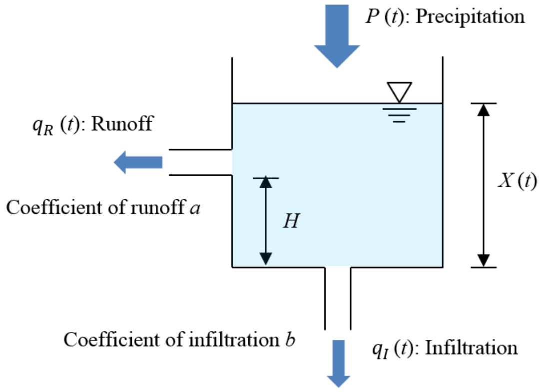

Figure 13 One-dimensional Tank Model

1) The equation of continuity shown by the equation (8) should be considered as an equation of state.
2) The equation below should be an observation equation and the 10 min runoff measured at the slope toe is used as an observation value for inverse analysis.

$$q_R(t)=a\cdot[X(t)-H] \tag{9}$$

In the analysis, the water level in a tank H, which is related to the surface retention generated immediately after the start of rainfall, is set at "H=2.7mm" based on the relationship between the cumulative rainfall and the runoff shown in Figure 14.

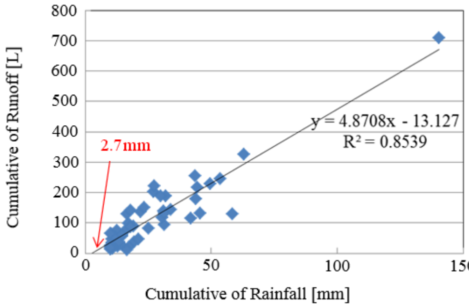

Figure 14 Correlation of cumulative rainfall amount and runoff amount

4.2 Simulation results of runoff and infiltration

By applying the rainfall data to the inverse analysis method, the analysis parameters were identified, and simulation of the runoff and the infiltration was carried out. As results of the simulation, Figure 15(a) and (b) show combined plot of measured and calculated values for the rainfall with the higher 10 min rainfall (13.5 mm) observed on October 17, 2012 and the rainfall with the smaller 10 min rainfall (5.0 mm) observed on November 24, 2012, and Figure 15(c) shows the correlation of the results. The simulation results show good agreement with measured values.

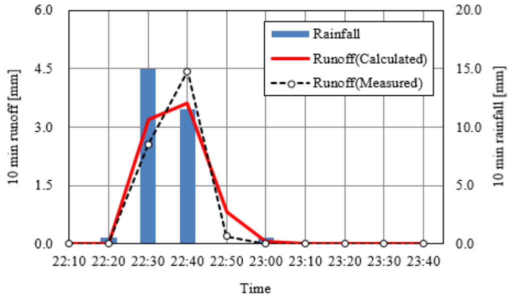

(a) October 17, 2012

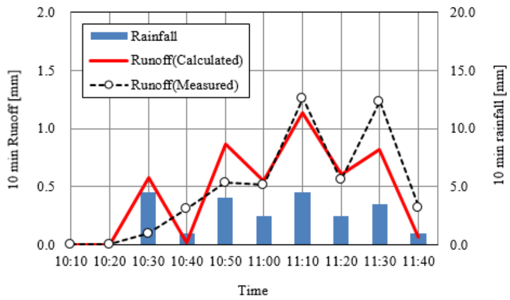

(b) November 24, 2012

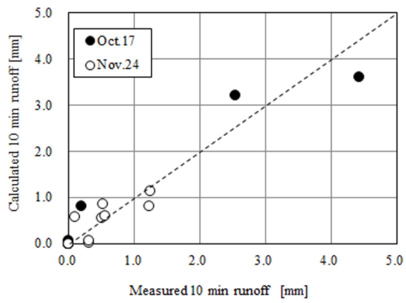

(c) Correlation of values for measured values and calculated values

Figure 15 Results of inverse analysis

Figure 16(a) and (b) show the correlation of the maximum 10 min rainfall, $(r_{10})_{MAX}$ and the identified coefficients of runoff and infiltration. While the coefficients of runoff shown in Figure 16(a) decrease with the increase of the maximum 10 min rainfall, the coefficients of infiltration shown in Figure 16(b) increase with the increase of the maximum 10 min rainfall. As shown in Figure 11, the runoff amount is dependent on the rainfall amount. The results in Figure 16 however indicate that the time rates of the runoff and infiltration may be dependent on the rainfall intensity.

Rainfall satisfies the capacity for initial abstraction and infiltration before a significant runoff can be produced (Overton & Meadows, 1976; Linsley et al, 1982). According to Premchitt et al (1992), the variation with the time rate and the cumulative amount of the components for a constant rainfall is summarized as follows: The initial abstraction consumes most or all of the initial rainfall, while it is insignificant at higher rainfall. Infiltration is large initially and gradually decline at high rainfall. Because the rainfall is largely absorbed by these two processes initially, there is a very small runoff at the start of rainstorm or for a light rain event. At higher rainfall, there is more runoff at a rate which is lower than the rainfall intensity, and the loss at this time will be the infiltration at the limiting rate.

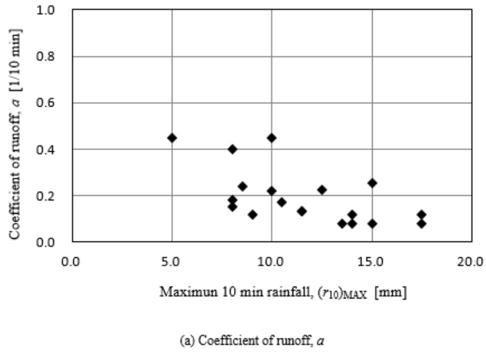

(a) Coefficient of runoff, a

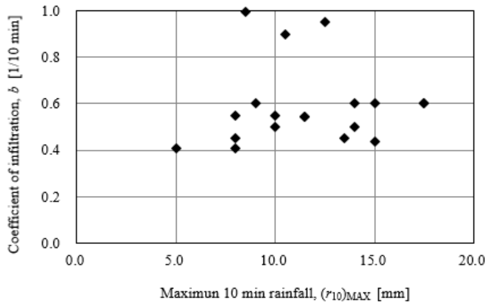

(b) Coefficient of infiltration, b

Figure 16 Identified Tank model parameters

Figure 17 to 19 show the variation with the time rate and the cumulative amount of rainfall, runoff and infiltration for three rainfalls observed on October 17, November 24 and September 18, respectively. At the rainfall with relatively higher-intensity shown in Figure 17, because the coefficients of the infiltration increase with the increase of the rainfall intensity shown in Figure 18, the infiltration is relatively larger and the runoff is produced immediately. The ratio of surface retention to other components is relatively small and the surface retention is partially transferred to the infiltration in a short period. On the other hand, at the rainfall with relatively smaller-intensity shown in Figure 16(b), the infiltration is small and the runoff is produced with time lag. The ration of surface retention is relatively large and is partially transferred to the infiltration with time lag. The above results for variable rainfall intensity are quite identical to the above findings presented by Premchitt, et al (1992).

In the comparison of Figure 17 with Figure 19, while the rainfall amount observed on October 17 is almost same as that on September 18, the variation with time rate and the cumulative amount of the components for the two rainfall records shows some differences. At the rainfall with the higher intensity, the infiltration is larger and the runoff is produced more swiftly. Furthermore, the surface retention is larger and is partially transferred to the infiltration more swiftly. The comparison therefore indicates that the time rates of the runoff and infiltration is heavily dependent on the rainfall intensity. The findings discussed in this section are verified by numerical analysis in next section

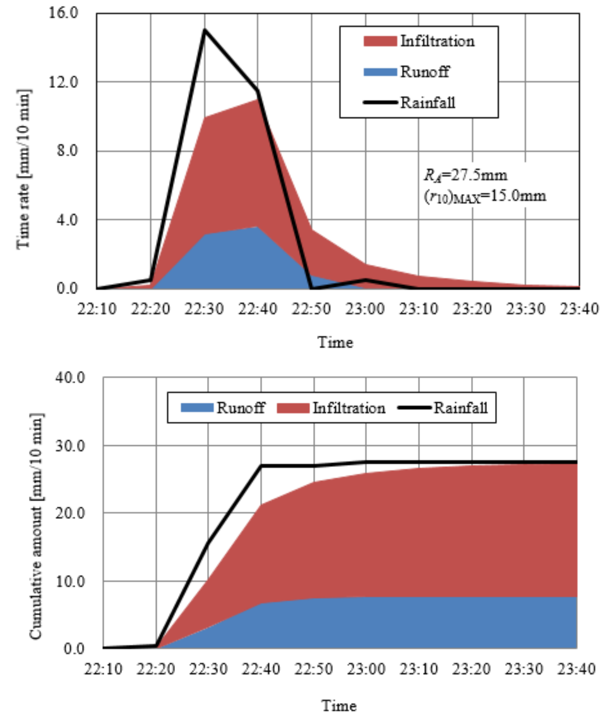

Figure 17 Time rate and the cumulative amount of rainfall, runoff and infiltration (October 17, 2012)

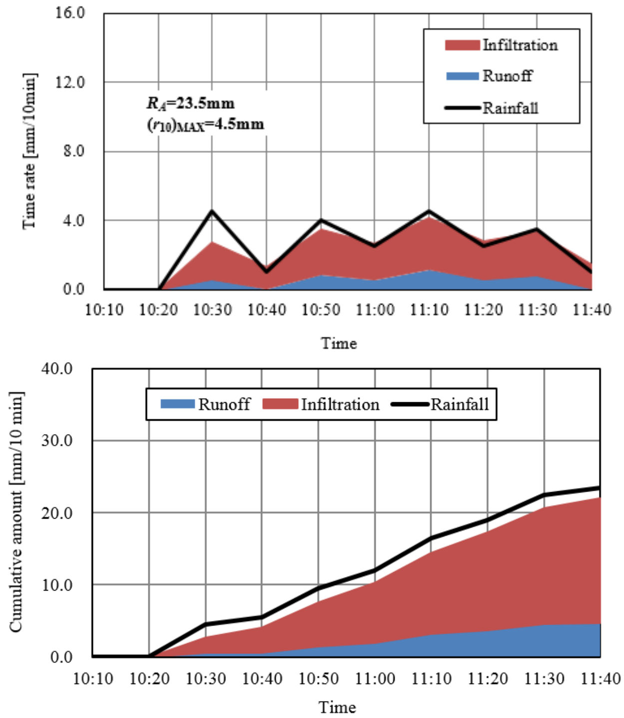

Figure 18 Time rate and the cumulative amount of rainfall, runoff and infiltration (November 24, 2012)

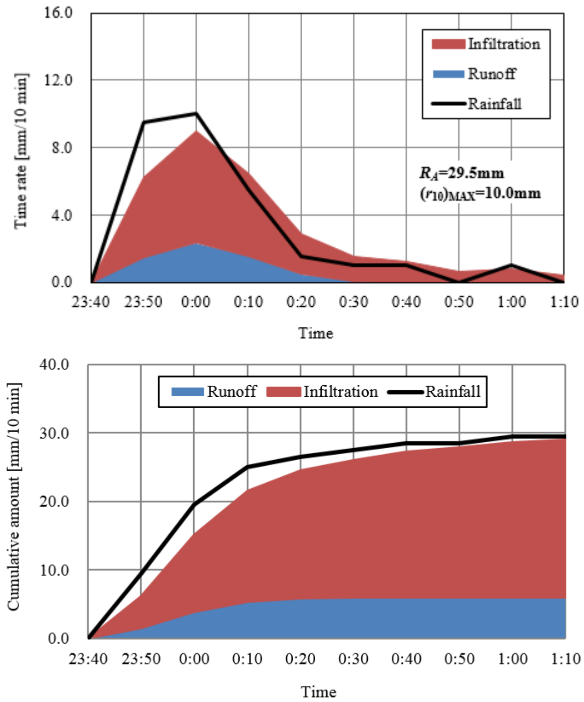

Figure 19 Time rate and the cumulative amount of rainfall, runoff and infiltration (September 18, 2012)

5. SEEPAGE ANALYSIS

In this section, the applicability of the proposed method for saturated-unsaturated seepage analysis, in which the infiltration obtained by the one-dimensional tank model is set as the prescribed flux boundary condition, is investigated, in comparison with the measured results and the results of the conventional method (Neuman, 1981).

5.1 Overview of analysis

As described in Section 1, infiltration has been conventionally evaluated indirectly by the conventional method in an analytical manner (Neuman, 1981). That is, it is assumed that in the analysis of the conventional method, the infiltration amount becomes larger at the initial stage compared to the infiltration amount calculated by the one-dimensional tank model and the infiltration by the conventional method does not continue so long as infiltration in the model.

5.2 Governing equation

The governing equation of a saturated-unsaturated seepage analysis is shown as follows (Neuman, 1981).

$$\mathrm{div}K(\theta)\vec{\nabla}(\psi+z)=\left(c(\psi)+AS_S\right)\frac{\partial\psi}{\partial t} \tag{10}$$

i=1,2,3 (1:x, 2:y, 3:z)

In which, $K(\theta)$ denotes hydraulic conductivity, θ denotes volumetric water content, ψ denotes pressure head, z denotes vertical coordination, S_S denotes coefficient of specific storage, $c(\psi)$ denotes specific water capacity. A represents 1 at saturated zone and represents 0 at unsaturated zone. In this study, commercial software named "3D-Flow" was adopted.

5.3 Modeling and Analysis condition

The model and analysis mesh are shown in Figure 20 which is corresponding to survey the line 4 shown in Figure 2. FE-mesh consists of 2,709 elements and 5,614 nodes. In this study, van Genuchten model were used to model the behavior for unsaturated region.

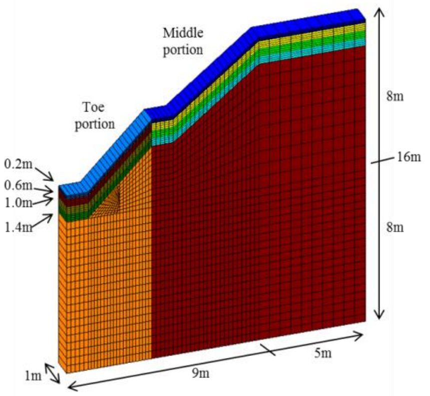

Figure 20 Analytical domain and FE-mesh of seepage analysis

Based on the comparison with the results of field measurement shown in Figure 12, the fitting suction-moisture curves for in-situ sampling date PK-01 and PK-32 shown in Figure 21(a) were adopted as the input data for the middle potion and the slope toe, respectively.

The hydraulic conductivity $K(\theta)$ shown in equation (8) is determined in accordance with the following equation (van Genuchten,1980):

$$K(\theta) = k_s Se^{\frac{1}{2}}\left[1-\left(1-Se^{1/m}\right)^m\right]^2 \tag{11}$$

In which, k_s denotes saturated coefficient of permeability.

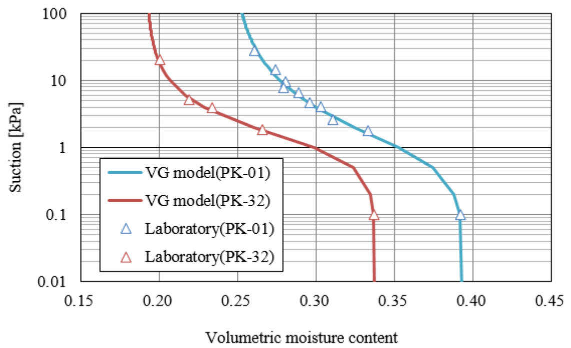

(a) Correlation of volumetric moisture content and suction

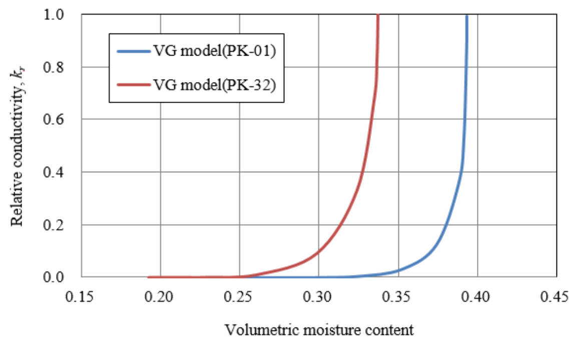

(b) Correlation of volumetric moisture content and specific hydraulic conductivity

Figure 21 SWCC used in seepage analysis

Figure 21(b) also shows the correlations of the volumetric moisture content and the relative hydraulic conductivity, k_r, which is the ratio of the hydraulic conductivity to the saturated coefficient of permeability, for in-situ sampling date PK-01 and PK-32. The parameters of the curves are set up based on the identified parameters as well as the suction-moisture curves. Table 3 shows the saturated coefficient of permeability used in this analysis, which are determined based on the result of in-situ investigations (see Table 2).

Table 3 Saturated coefficient of permeability

Depth	0.0~0.2m	0.2~0.6m	0.6~1.0m	1.0~1.4m	1.4m~
Middle	1.1×10^{-4}	4.0×10^{-5}	9.0×10^{-5}	1.0×10^{-5}	6.8×10^{-6}
Toe	2.0×10^{-4}	9.0×10^{-5}	2.0×10^{-5}	1.0×10^{-5}	5.3×10^{-6}

Unit: *m/s*

5.4 Results and consideration

Figure 22 and Figure 23 show the combined plot of the pore-water pressure in the field (at the middle portion of slope) and those obtained by both analyses for the rainfall events on October 17 and September 18.

As Figure 22 indicates, when the results at GL-0.2m are compared, the pore-water pressure of both analysis methods increased with the measured values at the almost same time. There is little difference in the variation of each result. In the same way, the results at GL-0.6m and GL-1.0m show that both conventional method and proposed method had better consistency with measured values. It indicates that because the produced surface retention is partially transferred in a short period, the difference on the variation of the pore-water pressure is insignificant. Next, Figure 23 shows that, when the results at GL-0.2m are compared, the pore-water pressure of the conventional method increased earlier than the measured value. On the other hand, the pore-water pressure of the proposed method analysis increased with the measured values at the almost same time. In addition, when the results at GL-0.6m and GL-1.0m are also compared, while the pore-water pressure for the analysis of the conventional method increases earlier than the measured values, the results by the proposed method had better consistency with the measured values. It indicates that the surface retention affects the variation of the pore-water pressure significantly.

It is therefore assumed that the proposed method can directly express the infiltration in an appropriate manner. Therefore, when the effect of the surface retention is larger, the difference of the increasing start time of pore-water pressure between conventional method and proposed method became larger. And, the results of proposed method had better correlation with the measured values.

However, it should be noticed that because the catchment in the slope in this study was relatively small, the rainfall-runoff relation was analysed by using a one-dimensional tank model. Thus, the infiltration was assumed to be constant all over the catchment. In the case of a larger catchment, it is needless to say that the infiltration in the slope is expected to vary place by place. Therefore, it is essential to develop a method using a larger number of tanks depending on the size of the catchment in the future

6. CONCLUDING REMARKS

This paper discussed results of runoff and infiltration due to torrential rainfall observed in Phuket, Thailand. Findings obtained in this study would be summarized as follows:

1) It was found that the measured rainfall-runoff relationship for the slope in this study is very similar to those for the same type of slope (weathered granite cut slope with grass cover).

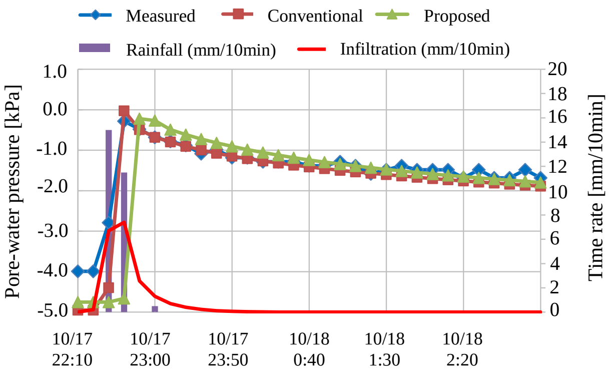

(a) GL-0.2m

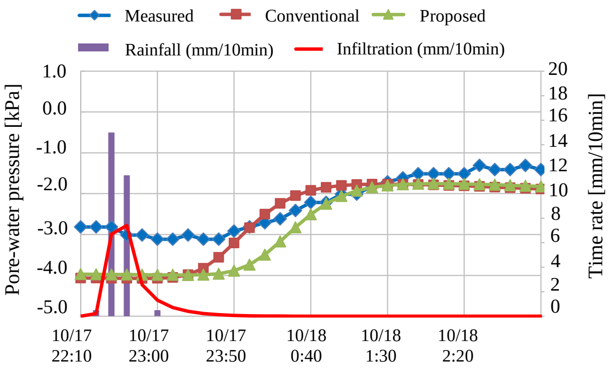

(b) GL-0.6m

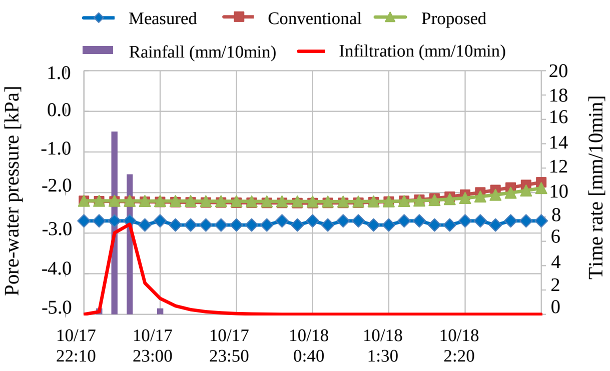

(c) GL-1.0m

Figure 22 Result of seepage flow analysis at Middle portion (Oct.17.2012)

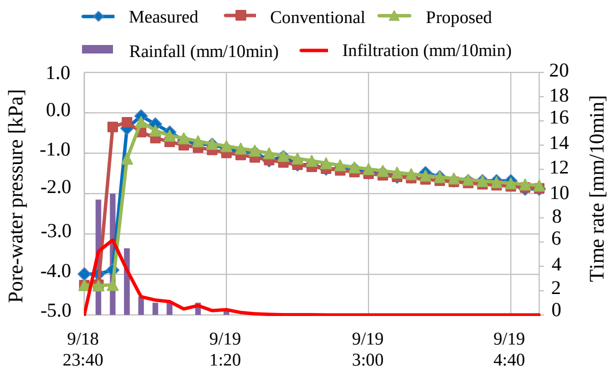

(a) GL-0.2m

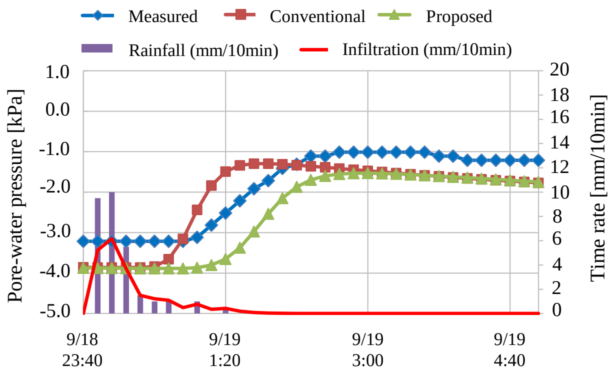

(b) GL-0.6m

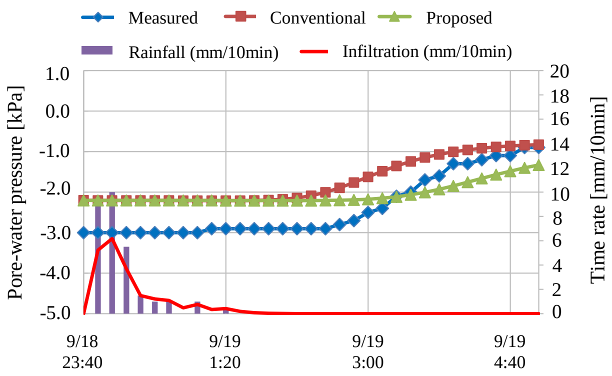

(c) GL-1.0m

Figure 23 Result of seepage flow analysis at Middle portion (Sep.18.2012)

2) The rainfall-runoff (Infiltration) is heavily dependent to rainfall intensity in addition to the rainfall amount. At the rainfall with relatively higher-intensity, because the coefficients of the infiltration increase with the increase of the rainfall intensity, the infiltration is relatively larger and the runoff is produced immediately. The surface retention is partially transferred to the infiltration in a short period. On the other hand, at the rainfall with relatively smaller-intensity, the infiltration is smaller and the runoff is produced with time lag. The surface retention is partially transferred to the infiltration gradually with time lag.

3) The results of the simulation for the variation of pore-water pressure showed that the proposed method in this study which deals with the infiltration simulated by one-dimensional tank model analysis as a prescribed flux boundary is applicable, by comparing with the measured values and the results of conventional method.

7. REFERENCES

Bujang, B. K. H., Faisal Hj. A, and Abdullah, A. (2005) Filed and laboratory suction-soil moisture relationship of unsaturated residual soil, American Journal of Environmental Science 1 (1), pp34-40.

Dearman, W. R., Baynes, F. J. and Irfan, T, Y. (1978) Engineering grading of weathered granite, Engineering Geology, 12, pp345-374.

Fredlund, D. G. and & Rahardjo, H. (1993), Soil Mechanics for Unsaturated Soils, New York: Jon Wiley and Sons Inc.

Geological Society Engineering Group Working Party Report (1994) Tropical residual soils, Quarterly Journal of Engineering Geology, 11, pp233-244.

GCO (1984) Geotechnical Manual for Slopes 2nd Edition, Geotechnical Control Office, Engineering Development Department, Hong Kong, p295.

Horton, E. R. (1940) An approach toward a physical interpretation of infiltration-capacity, Soil Sci. Soc. Am., Proc. 5, pp399-417.

Inoue, M. (1994) Underground soil suction sensor", Sand Dune Research, Vol.41, No.2, pp74-79.

Jworcha, I. (2006) Minerology and chemical properties of residual soils, IAEG2006 Paper number 21, The Geological Society of London 2006.

Linsley, R.K., Kohler, M.A. and Paulhus, J.L.H. (1982) Hydrogy for Engineers (Third edition), McGraw-Hill, New York, p508.

Little, A.L. (1969) The engineering classification of residual tropical soils, Proceedings 7th International Conference on Soil Mechanics and Foundation Engineering, Mexico 1, pp1-10.

Matsushi, Y. (2006) Triggering mechanisms and rainfall thresholds of shallow landslides on soil-mantled hill slopes with permeable and impermeable bedrocks, Ph.D. Dissertation of the University of Tsukuba.

Neuman, S. P. (1974) Galerkin Approach to Unsaturated Flow in Soils, Finite Element Methods in Flow Problems, UAH Press, University of Alabama in Huntsville, pp517-522.

Ohtsu, H., Ikenaga, J. and Takahashi, K. (2013) A Study on Applicability of Various Precipitation Indexes Considering the Characteristic of Runoff-Infiltration near Slope Surface, Proceedings of EIT-JSCE Joint Symposium 2013, on CD.

Overton, D.E. and Meadows, M.E. (1976) Storm Modelling, Academic Press, New York, p358.

Premchitt, J., Lam, T.S.K., Shen, J.M. & Lam, H.F. (1992) Rainstorm Runoff on Slopes (GEO Report No. 12), Geotechnical Engineering Office, Hong Kong, pp1-104.

Phien-Wej, N., Nutalaya, P., Aung, Z. and Zhibin, T. (1993) Catastrophic Landslides and Debris Flows in Thailand, ENGINEERING GEOLOGY, No.48, pp93-100.

Seki, K. (2007) SWRC fit - a nonlinear fitting program with a water retention curve for soils having unimodal and bimodal pore structure, Hydrol. Earth Syst. Sci. Discuss., 4, pp407-437.

Soil Conservation Service (1972) National Engineering Handbook, Section 4: Hydrology, Soil Conservation Service, United States Department of Agriculture, Washington, D.C.

Soralump, S. (2010) Rainfall-Triggered Landslide: from research to mitigation practice in Thailand, Geotechnical Engineering Journal of the SEAGS &AGSSEA, Vol. 41, No.1.

Sugawara, M. (1995) Tank model Computer models of watershed hydrology, V. P. Singh, ed., Water Resources Publications, Littleton, Colorado.

Suwanishwong, T., Ohtsu, H. and Takahashi, K. (2008) Application of Kalman filter algorithm in Parameters identification of modified Multi Tank Model system, Journal of the Southeast Asian Geotechnical Society, pp113-121.

Van Genuchten, M. (1980) A closed equation for predicting the hydraulic conductivity of unsaturated soils", Soil Sci. Soc. Am. Proc., 44, pp892-898.